Supporting Information

Integrating the atomically separated frontier molecular orbital distribution of two multiple resonance frameworks through a single bond for high-efficiency narrowband emission

Meng-Yuan Chen, ‡[a] Feng Huang, ‡[a] Hao Wu,[a] Ying-Chun Cheng,[a] Hui Wang,[a] Ya-Nan Hu,[a] Xiao-Chun Fan,[a] Jia Yu,[ab] Kai Wang,[ac*] Xiao-Hong Zhang [ab*]

[a] *Institute of Functional Nano & Soft Materials (FUNSOM), Soochow University, Suzhou, Jiangsu 215123, P. R. China*

[b] *Jiangsu Key Laboratory of Advanced Negative Carbon Technologies, Soochow University, Suzhou, Jiangsu 215123, P. R. China*

[c] *Jiangsu Key Laboratory for Carbon-Based Functional Materials & Devices, Soochow University, Suzhou, Jiangsu, 215123, P. R. China*

‡ *These authors contributed equally to the work.*

*E-mail: wkai@suda.edu.cn

*E-mail: xiaohong_zhang@suda.edu.cn

Content

General Information

Materials. ^{1}H NMR and ^{13}C NMR spectra were recorded on a Bruker 600 spectrometer at room temperature. Mass spectra were recorded on a Thermo ISQ mass spectrometer using a direct exposure probe.

Measurement of absorption and emission characteristics. UV–vis absorption spectra were recorded on a Hitachi U-3900 spectrophotometer. PL spectra were recorded on a Hitachi F-4600 fluorescence spectrophotometer. PL quantum efficiencies were measured by an absolute PL quantum yield measurement system (C11347-01, Hamamatsu Photonics) under the flow of nitrogen gas with an excitation wavelength of 300 nm. Transient PL decay was measured using an Edinburgh fluorescence spectrometer (FLS920) under vacuum.

Thermal and electrochemical measurements. Thermogravimetric analysis (TGA) curves were obtained on a Perkin Elmer at a heating rate of 10 $°C \cdot min^{-1}$ from 0 to 800 °C under nitrogen. The temperature of 5% weight loss was defined as the decomposition temperature (T_d). Differential scanning calorimetry (DSC) curves were obtained on a TA DSC 2010 unit at a heating rate of 10 $°C \cdot min^{-1}$ from 0 to 350 °C under nitrogen. Cyclic voltammetry (CV) was carried out on a CHI660E electrochemical analyser using a silver/silver chloride (Ag/AgCl) electrode as the reference electrode and Pt disks as the working electrode and the counter electrode. In the experiments, 0.1 M tetrabutylammonium perchlorate in 10^{-3} M dichloromethane solution was used as the supporting electrolyte, and ferrocene/ferrocenium (Fc/Fc^{+}) served as the internal reference with a scan rate of 0.1 V/s under a nitrogen atmosphere.

Theoretical calculations. All the calculations are performed using the Gaussian 09 program package. Theoretical calculations of the ground state are performed by using density functional theory (DFT) at the level of B3LPY/6-31G (d). Natural transition orbitals (NTOs) of the lowest adiabatic excited states were analysed via a multifunctional wavefunction analyser (Multiwfn 3.6).

Angle-dependent PL measurement. The angle-dependent PL spectra were measured through a molecular orientation characteristic measurement system (C14234-11, Hamamatsu Photonics). The thin films were fabricated by vacuum thermal deposition on a glass substrate and encapsulated with a coverslip under a nitrogen atmosphere. The PL intensity in transverse magnetic mode was detected by a monochromator (PMA-11, Hamamatsu Photonics). The PL intensities were acquired at each out-of-plane angle from 0° (vertical to the substrate surface) to 90° (horizontal to the substrate surface). The obtained PL intensity angle-dependent patterns were analysed using a software package (U6039-09 Ver1.1.0 for C14234). The horizontal dipole ratio ($\Theta_{//}$) is defined by the equation $\Theta_{//} = p_{//}/(p_{//} + p_{\perp})$, in which $p_{\perp}$ and $p_{//}$ are the transition dipole moments perpendicular and parallel to the substrate surface, respectively.

Device fabrication and measurement. OLEDs were fabricated on indium-tin oxide (ITO)-coated transparent glass substrates, and the ITO conductive layer had a thickness of ca. 100 nm and a sheet resistance of ca. 30 Ω per square. The substrates were cleaned with ethanol, acetone, and deionized water, dried in an oven, and finally exposed to UV ozone for 15 min. All of the organic materials and metal layers were thermally evaporated under a vacuum of ca. 10^{-5} Torr. Four identical OLED devices were formed

on each of the substrates, and the emission area was 0.1 cm^2 for each device. The EL performances of the devices were measured with a PHOTONIC MULTI-CHANNEL ANALYZER PMA-12 with an integrating sphere and a KEITHLEY 2400 Source Meter constant current source at room temperature.

Experimental

Synthesis

DOBNA-Bpin, *m*-Br-BNCz and *p*-Br-BNCz were synthesized according to previously reported literature. Other chemicals and reagents used in this work were purchased commercially without further purification.

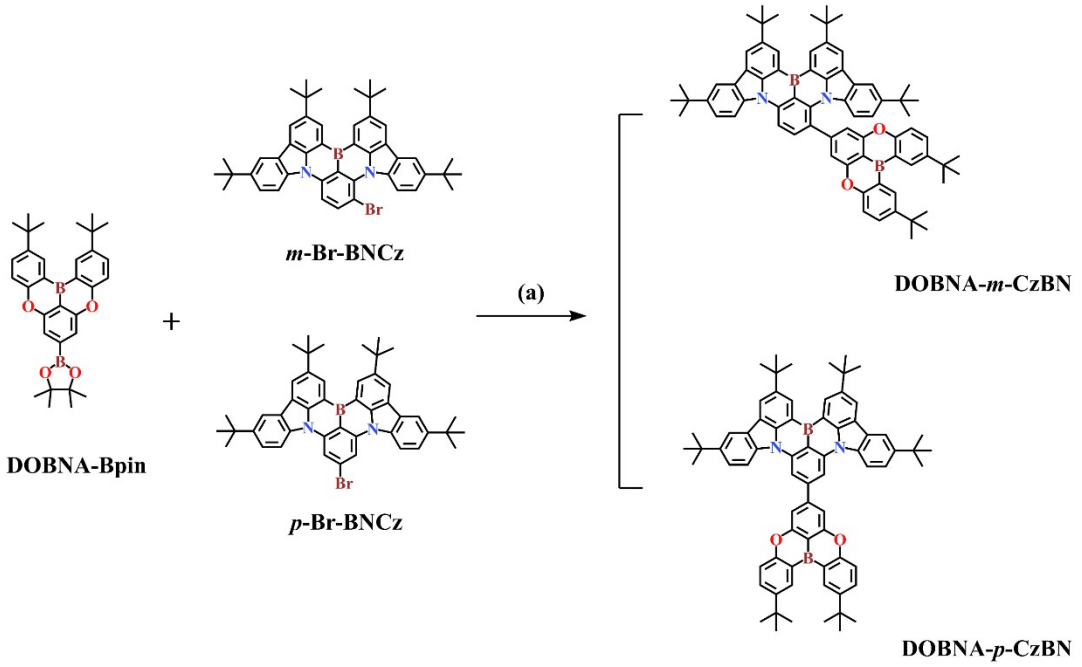

Scheme S1. Synthetic routes for DOBNA-*m*-CzBN and DOBNA-*p*-CzBN. (a) $Pd(PPh_3)_4$, K_2CO_3, Dioxane. Refluxed at 110 °C under N_2 protection.

Synthesis of **DOBNA-Bpin**: The synthesis process was performed according to the reported literature.[1, 2]

Synthesis of ***m*-Br-BNCz** and ***p*-Br-BNCz**: The synthesis process was performed according to the reported literature.[3, 4]

Synthesis of **DOBNA-*m*-CzBN**: A mixture of *m*-Br-BNCz (1.44 g, 2 mmol), DOBNA-Bpin (1.12 g, 2.2 mmol), $Pd(PPh_3)_4$ (115.59 mg, 0.1 mmol) potassium carbonate aqueous solution (4 mL, 1 M) and 100 mL dioxane were added to a 250 mL two-neck flask under nitrogen protection and then refluxed at 110 °C for 12 h. After cooling the reaction to room temperature, the mixture was filtered with crude silica gel and then evaporated under reduced pressure. The crude product was purified by column chromatography (eluent: petroleum ether and dichloromethane) and obtained as a yellow powder (455 mg, 0.45 mmol, yield: 22%). ^{1}H NMR (400 MHz, Chloroform-*d*) δ 9.10 (dd, J = 8.4, 1.6 Hz, 2H), 8.80 (d, J = 2.4 Hz, 2H), 8.52 (dd, J = 15.2, 1.7 Hz, 2H), 8.35 (d, J = 1.9 Hz, 1H), 8.24 (d, J = 1.9 Hz, 1H), 8.17 (d, J = 8.9 Hz, 1H), 7.88 — 7.83 (m, 2H), 7.74 (dd, J = 8.8, 2.4 Hz, 2H), 7.52 (dd, J = 8.8, 2.0 Hz, 1H), 7.40 (d, J = 8.8 Hz, 2H), 7.31 (s, 2H), 6.98 (d, J = 8.3 Hz, 1H), 6.90 (s, 1H), 1.71 (d, J = 4.7 Hz, 18H), 1.63 (s, 9H), 1.50 (d, J = 6.1 Hz, 27H). ^{13}C NMR (101 MHz, Chloroform-*d*) δ 162.55, 158.77, 157.72, 148.38, 146.09, 145.00, 144.90, 144.59, 143.18, 142.01, 141.62, 138.35, 135.42, 131.36, 130.01, 129.82, 128.97, 128.09, 127.79, 126.82, 124.28, 123.69, 123.61, 120.71, 120.37, 118.15, 117.03, 116.89, 114.11, 112.07, 108.15, 107.97, 36.50, 35.24, 35.17, 34.98, 34.71, 34.55, 32.25, 32.22, 31.94, 31.78, 31.56, 31.45, 29.71, 29.33. MALDI-TOF MS (mass m/z): 1020.9488 $[M]^+$; calcd for $C_{72}H_{74}B_2N_2O_2$ 1020.5936.

Synthesis of **DOBNA-*p*-CzBN**: A mixture of *p*-Br-BNCz (1.44 g, 2 mmol), DOBNA-Bpin (1.12 g, 2.2 mmol), $Pd(PPh_3)_4$ (115.59 mg, 0.1 mmol), potassium carbonate aqueous solution (4 mL, 1 M) and 100 mL dioxane were added to a 250 mL two-neck

flask under nitrogen protection and then refluxed at 110 °C for 12 h. After cooling the reaction to room temperature, the mixture was filtered with crude silica gel and then evaporated under reduced pressure. The crude product was purified by column chromatography (eluent: petroleum ether and dichloromethane) and obtained as a yellow powder (558 mg, 0.53 mmol, yield: 27%). ^{1}H NMR (400 MHz, Chloroform-*d*) δ 9.09 (d, J = 1.9 Hz, 2H), 8.78 (d, J = 2.6 Hz, 2H), 8.57 (s, 2H), 8.48 — 8.43 (m, 4H), 8.25 (d, J = 2.1 Hz, 2H), 7.80 (dd, J = 8.8, 2.4 Hz, 2H), 7.73 (d, J = 10.1 Hz, 4H), 7.57 (d, J = 8.7 Hz, 2H), 1.70 (s, 18H), 1.57 (s, 18H), 1.55 (s, 18H). ^{13}C NMR (151 MHz, Chloroform-*d*) δ 158.79, 157.92, 145.24, 145.16, 144.96, 144.55, 144.51, 141.67, 138.21, 131.43, 130.21, 129.67, 127.05, 124.57, 123.60, 120.59, 117.99, 117.20, 114.22, 107.69, 107.32, 35.15, 34.80, 34.56, 32.19, 31.85, 31.58. MALDI-TOF MS (mass m/z): 1020.9794 $[M]^{+}$; calcd for $C_{72}H_{74}B_2N_2O_2$ 1020.5936.

Thermal measurements

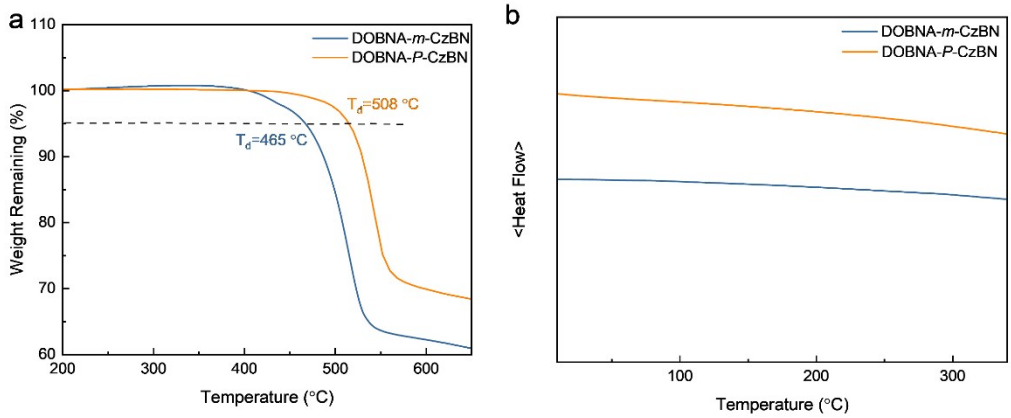

Figure S1. (a) TGA and (b) DSC traces for DOBNA-*m*-CzBN and DOBNA-*p*-CzBN.

Theoretical Calculations

a

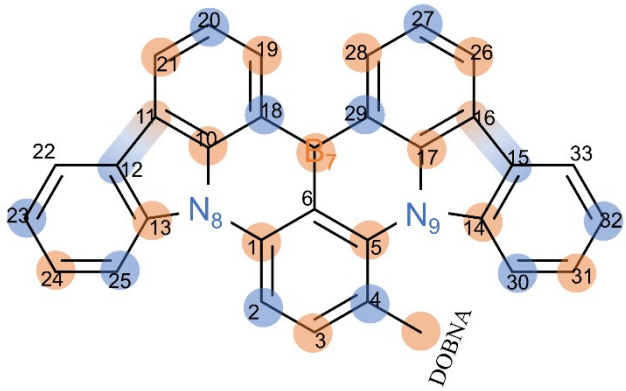

DOBNA-*m*-CzBN	HOMO		LUMO	
	Coefficient		Coefficient	
	2PZ	3PZ	2PZ	3PZ
C1	-0.09718	-0.0557	**-0.14323**	**-0.12293**
C2	**-0.20326**	**-0.16728**	-0.03957	-0.05247
C3	0.01811	0.01433	**0.16418**	**0.17872**
C4	**0.23017**	**0.1853**	-0.02903	-0.05485
C5	0.09041	0.06618	**-0.1412**	**-0.13245**
C6	-0.00279	-0.01045	0.04187	0.03823
B7	0.00066	-0.00511	**0.26042**	**0.25775**
N8	**0.22046**	**0.1905**	0.07059	0.0768
N9	**-0.20316**	**-0.17773**	0.06488	0.0717
C10	-0.0456	-0.03586	**-0.06646**	**-0.05397**
C11	**-0.08279**	**-0.06533**	**-0.10928**	**-0.12358**
C12	**-0.07896**	**-0.06215**	**-0.08421**	**-0.07313**
C13	-0.01701	-0.00468	**0.0969**	**0.07535**
C14	0.02175	-0.00127	**0.0658**	**0.05396**

C15	**0.06414**	**0.06004**	**-0.06316**	**-0.06473**
C16	**0.07973**	**0.06296**	**-0.0974**	**-0.10838**
C17	0.04755	0.04206	**-0.06377**	**-0.05282**
C18	**-0.12485**	**-0.09769**	0.05385	0.05109
C19	-0.015	-0.01557	**-0.18494**	**-0.18707**
C20	**0.11599**	**0.09576**	0.02418	0.01671
C21	0.07393	0.05646	**0.18636**	**0.19959**
C22	0.05164	0.03728	0.05399	0.05719
C23	**0.09924**	**0.08333**	0.04842	0.05494
C24	-0.00445	-0.00663	**-0.08046**	**-0.08873**
C25	**-0.09507**	**-0.0726**	-0.01005	-0.0055
C26	-0.06971	-0.05398	**0.16111**	**0.16869**
C27	**-0.11008**	**-0.09203**	0.02468	0.01224
C28	0.01378	0.01826	**-0.16171**	**-0.15236**
C29	**0.12625**	**0.10304**	0.04392	0.03652
C30	**0.07167**	**0.04949**	-0.0086	-0.0031
C31	0.00221	0.00394	**-0.06107**	**-0.06363**
C32	**-0.08634**	**-0.07073**	0.03549	0.04011
C33	-0.04531	-0.03446	0.04368	0.04471

b

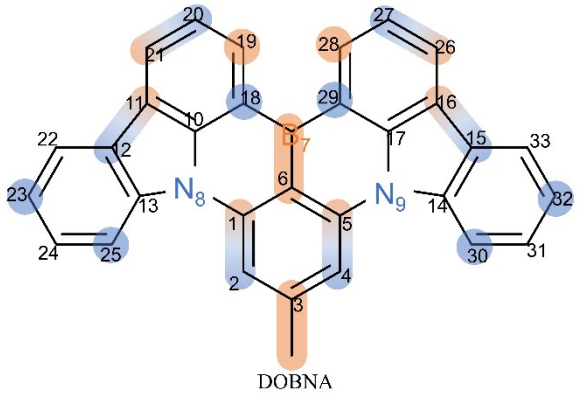

DOBNA-*p*-CzBN	HOMO		LUMO	
	Coefficient		Coefficient	
	2PZ	3PZ	2PZ	3PZ
C1	**-0.08454**	**-0.06395**	**-0.11832**	**-0.10764**
C2	**-0.21529**	**-0.16604**	**-0.07046**	**-0.07364**
C3	0	0	**0.15368**	**0.15118**
C4	**0.21529**	**0.16604**	**-0.07046**	**-0.07364**
C5	**0.08454**	**0.06395**	**-0.11832**	**-0.10764**
C6	0	0	**0.07923**	**0.09009**
B7	0	0	**0.18959**	**0.18862**
N8	**0.23834**	**0.19712**	0.06529	0.06822
N9	**-0.23834**	**-0.19712**	0.06529	0.06822
C10	-0.05817	-0.0415	-0.05775	-0.03893
C11	**-0.08182**	**-0.06325**	**-0.07359**	**-0.08731**
C12	**-0.07871**	**-0.06096**	-0.05452	-0.04544
C13	-0.02249	-0.01254	0.06779	0.05072

C14	0.02249	0.01254	0.06779	0.05072
C15	**0.07871**	**0.06096**	-0.05452	-0.04544
C16	**0.08182**	**0.06325**	**-0.07359**	**-0.08731**
C17	0.05817	0.0415	-0.05775	-0.03894
C18	**-0.12931**	**-0.10283**	0.02458	0.0258
C19	-0.01515	-0.01653	**-0.12728**	**-0.12904**
C20	**0.1237**	**0.10131**	0.02611	0.0202
C21	**0.08036**	**0.06147**	**0.12744**	**0.13611**
C22	0.05712	0.0435	0.03365	0.03275
C23	**0.10603**	**0.08628**	0.0347	0.03946
C24	-0.00583	-0.01194	-0.04994	-0.05412
C25	**-0.0954**	**-0.06925**	-0.01125	-0.0106
C26	**-0.08036**	**-0.06147**	**0.12744**	**0.13611**
C27	**-0.1237**	**-0.10131**	0.02611	0.0202
C28	0.01515	0.01652	**-0.12728**	**-0.12904**
C29	**0.12931**	**0.10283**	0.02458	0.0258
C30	**0.0954**	**0.06924**	-0.01125	-0.0106
C31	0.00583	0.01194	-0.04994	-0.05412
C32	**-0.10603**	**-0.08628**	0.0347	0.03946
C33	-0.05712	-0.0435	0.03365	0.03275

Figure S2. The coefficients of the 2PZ/3PZ basis functions of (a) DOBNA-*m*-CzBN and (b) DOBNA-*p*-CzBN. The Z-axis is vertical to the sheet (π-plane).

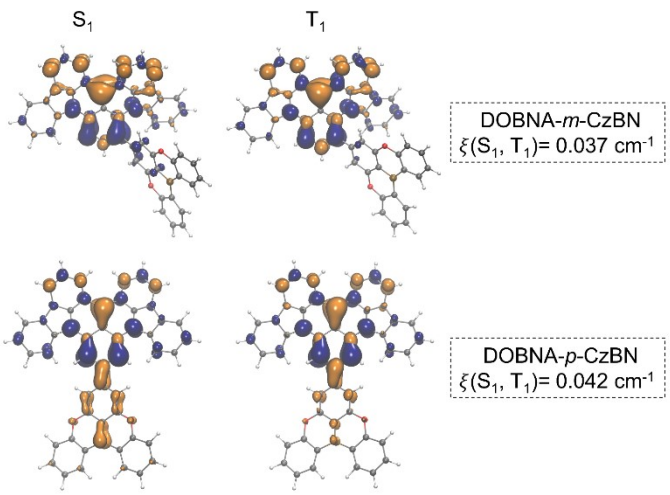

Figure S3 Calculated natural transition orbital (NTO) distributions of DOBNA-*m*-CzBN and DOBNA-*p*-CzBN in S_1 and T_1 states (yellow represents particles, blue represents holes) and their SOC matrix elements between S_1 and T_1.

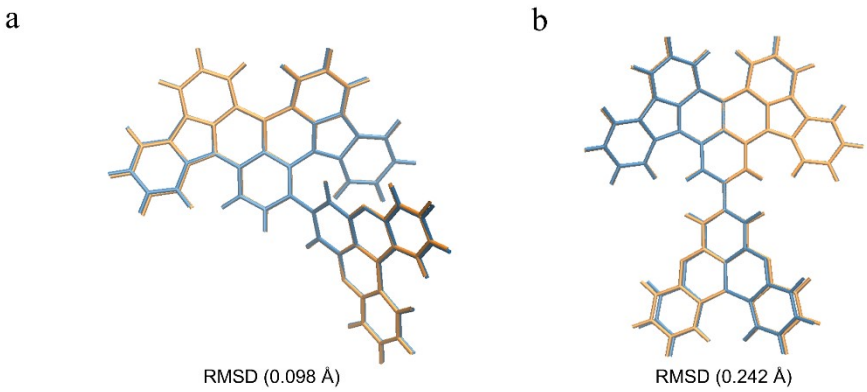

Figure S4. Geometry comparisons between the optimized S_0 and S_1 states of (a) DOBNA-*m*-CzBN and (b) DOBNA-*p*-CzBN via Multifun 3.7.

Electrochemical measurements

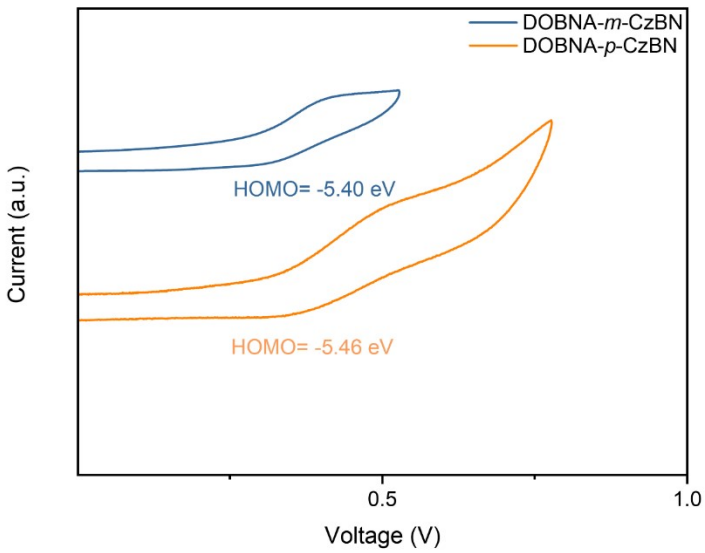

Figure S5. Cyclic voltammetry curves of DOBNA-*m*-CzBN and DOBNA-*p*-CzBN.

Photophysical Properties

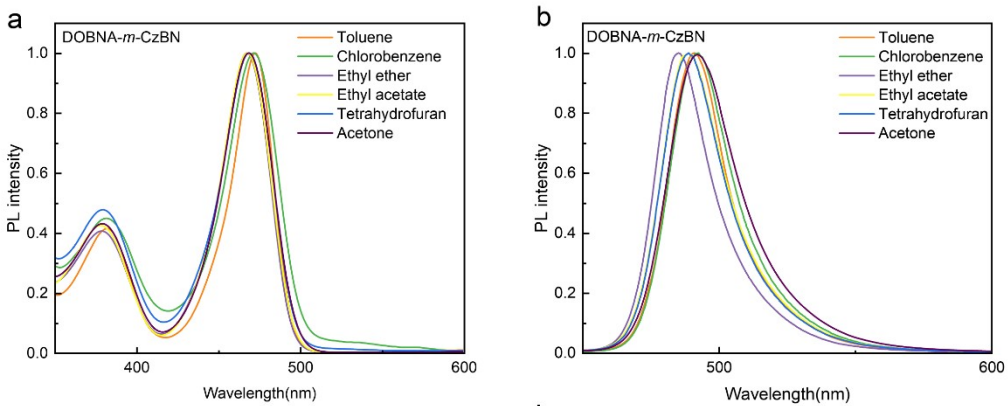

Figure S6. (a) UV–vis absorption and (b) fluorescence spectra of DOBNA-*m*-CzBN in different solvents.

Table S1. Detailed absorption and emission peak positions of DOBNA-*m*-CzBN in different solvents.

solvents[a)]	n[b)]	$f(\varepsilon, n)$[c)]	DOBNA-*m*-CzBN		
			λ_{abs}[d)] [nm]	λ_{em}[d)] [nm]	ν_a-ν_f[e)] [cm^{-1}]
Toluene	1.496	0.014	474	491	747
Chlorobenzene	1.524	0.143	474	492	771
Ethyl ether	1.352	0.167	469	485	737
Ethyl acetate	1.372	0.200	469	488	807
Tetrahydrofuran	1.407	0.210	470	489	826
Acetone	1.359	0.284	471	492	885

[a)] The solvent selected has good solubility to the emitters; [b)] the solvent refractive index; [c)] the orientational polarizability of the solvent; [d)] Peak wavelength of absorption and emission in different solvents; [e)] ν_a-ν_f=1/λ_{abs}-1/λ_{em}.

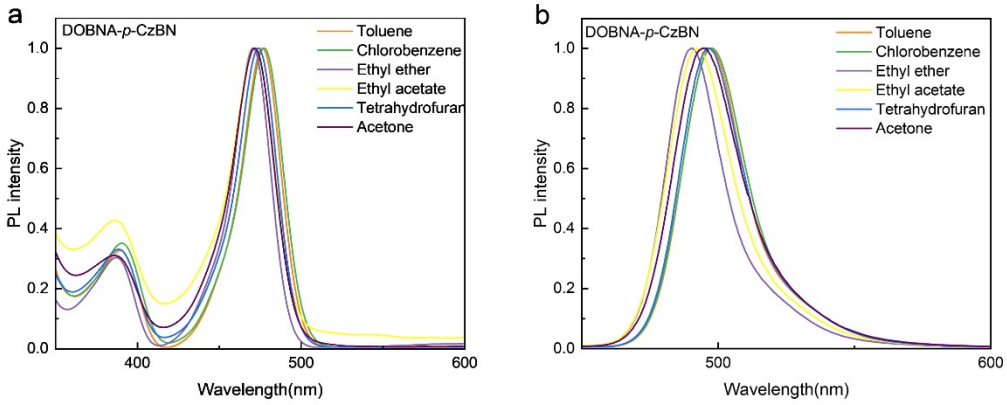

Figure S7. (a) UV–vis absorption and (b) fluorescence spectra of DOBNA-*p*-CzBN in different solvents.

Table S2. Detailed absorption and emission peak positions of DOBNA-*p*-CzBN in different solvents.

solvents	N	$f(\varepsilon, n)$	DOBNA-*p*-CzBN		
			λ_{abs} [nm]	λ_{em} [nm]	ν_a-ν_f [cm^{-1}]
Toluene	1.496	0.014	477	497	843
Chlorobenzene	1.524	0.142	478	497	824
Ethyl ether	1.352	0.167	470	490	885
Ethyl acetate	1.372	0.200	472	493	908
Tetrahydrofuran	1.407	0.210	475	497	945
Acetone	1.359	0.284	472	496	1025

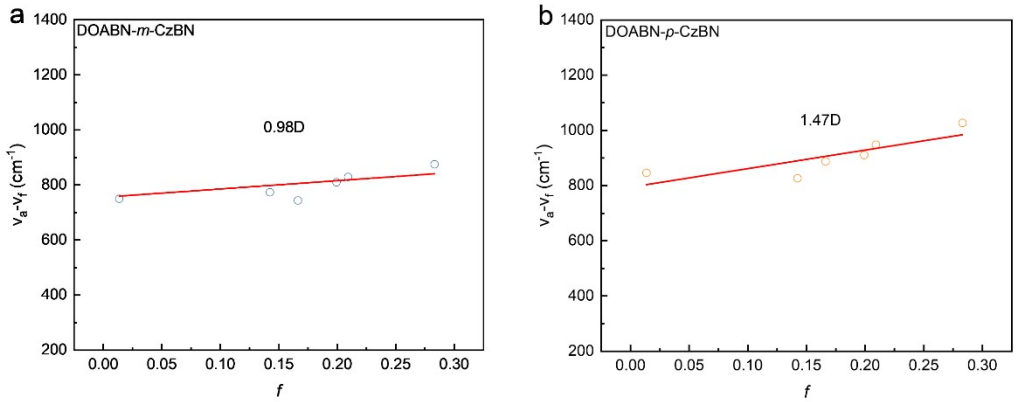

Figure S8. Linear correlation of the orientational polarization (*f*) of solvent media with the Stokes shift (v_a-v_f; a: absorbed light; f: fluorescence) for (a) DOBNA-*m*-CzBN and (b) DOBNA-*p*-CzBN. These results are based on the Lippert-Mataga equation fitted from the reported literature.[5]

Kinetic Analysis

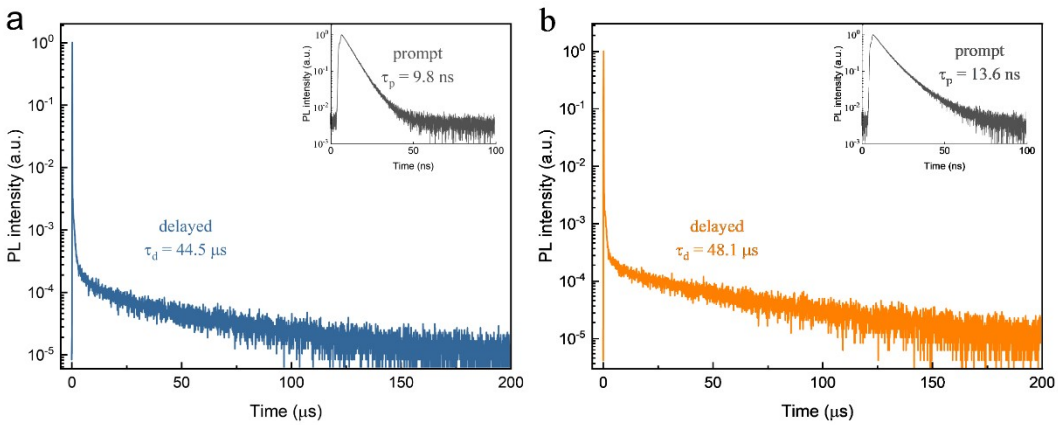

Figure S9. Transient fluorescence decay curves of the delayed emission and prompt emission for (a) DOBNA-*m*-CzBN and (b) DOBNA-*p*-CzBN with 3 wt% doped in PhCzBCz films.

The prompt lifetimes were obtained by exponential fitting of the prompt PL curves with a monoexponential function as $I_t = I_0 e^{\frac{-t}{\tau_p}}$, in which *I* is the photoluminescence intensity, t is the decay time, and τ_p is the prompt lifetime. Prompt and delayed fluorescence quantum efficiencies (Φ_p and Φ_d) were determined by using total PL quantum

efficiency (Φ_{PL}) and the relative ratios between prompt and delayed components, which were calculated from the following transient PL measurements.

As $k_{IC} << k_F$, k_{IC} can often be ignored, and nonradiative decay rates of triplet excitons (k_{nr}^T) are considered the main loss channel due to their long lifetime before decay. The key kinetic parameters of DOBNA-*m*-CzBN- and DOBNA-*p*-CzBN-doped films are calculated according to the following equations:

$$k_p = \frac{1}{\tau_p} \quad (1)$$

$$k_d = \frac{1}{\tau_d} \quad (2)$$

$$k_r^S = k_p \phi_p \quad (3)$$

$$k_{ISC} = k_p(1 - \phi_p) \quad (4)$$

$$k_{RISC} = \frac{k_p k_d \phi_d}{k_{ISC} \phi_p} \quad (5)$$

$$k_{nr}^T = k_d - \phi_p k_{RISC} \quad (6)$$

where k_p, k_{RISC}, and k_d are the rate constants of prompt fluorescence, RISC, and delayed fluorescence decay, respectively, and k_{nr}^T is the nonradiative decay rate constant of triplet excitons.

Table S3. Kinetic parameters of the emitters doped in PhCzBCz films.

Emitters	3 wt% in PhCzBCz									
	Φ_{PL} [%]	Φ_p/Φ_d [%]	τ_p [ns]	τ_d [μs]	k_p [10^8 s^{-1}]	k_d [10^4 s^{-1}]	k_r^S [10^7 s^{-1}]	k_{ISC} [10^7 s^{-1}]	k_{RISC} [10^4 s^{-1}]	k_{nr}^T [10^3 s^{-1}]
DOBNA-*m*-CzBN	96.2	71.2/25.0	9.8	44.5	1.0	2.2	7.2	2.9	2.7	3.0
DOBNA-*p*-CzBN	95.1	69.3/25.8	13.5	48.1	7.4	2.1	5.0	2.3	2.5	3.3

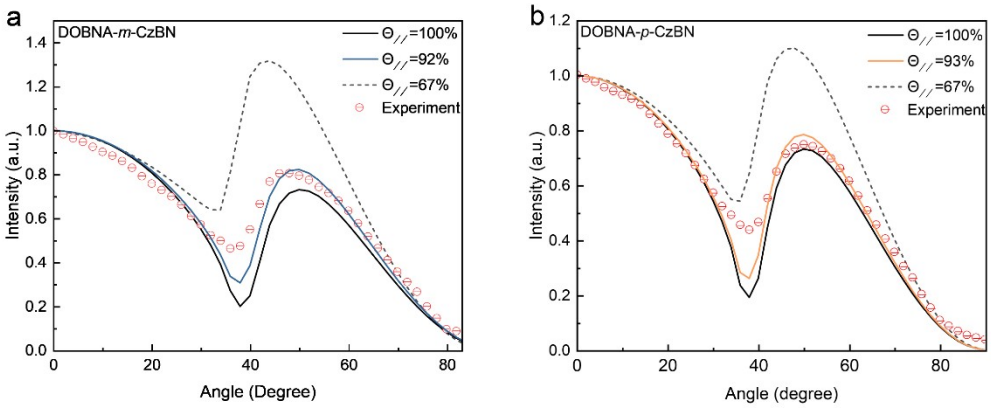

Figure S10. Angle-dependent PL intensity of p-polarized light from (a) DOBNA-*m*-CzBN and (b) DOBNA-*p*-CzBN 3 wt% doped in PhCzBCz films.

Device Characterization

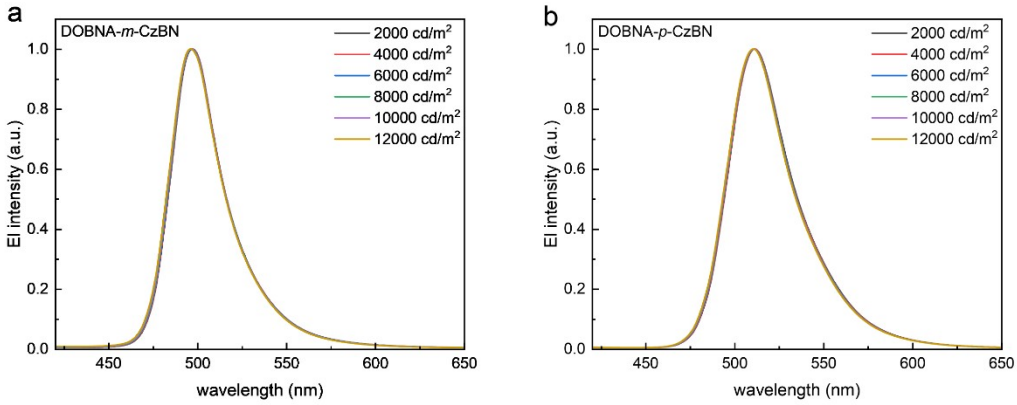

Figure S11. The EL spectra of (a) DOBNA-*m*-CzBN- and (b) DOBNA-*p*-CzBN-based OLEDs with 3 wt% doping in PhCzBCz varying with luminance.

Table S4. Electroluminescence properties of DOBNA-*m*-CzBN-based devices.

Concentration wt%	λ_{em} [nm]	FWHM [nm]/[meV]	CE_{max} [cd A^{-1}]	PE_{max} [lm W^{-1}]	EQE_{max}/EQE_{1000} [%]	CIE (x, y)
1	495	28/145	55.4	51.2	34.5/11.3	(0.11, 0.49)
3	497	28/141	91.5	84.5	38.6/15.7	(0.11, 0.54)
5	498	29/148	82.8	72.2	35.5/16.3	(0.11, 0.56)
7	498	29/149	84.5	73.7	34.8/18.1	(0.11, 0.56)

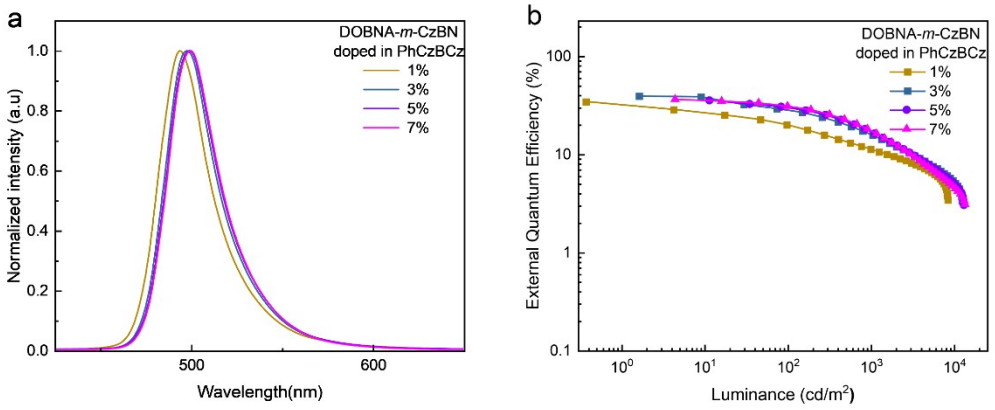

Figure S12. OLED device performances for DOBNA-*m*-CzBN with different doping concentrations. (a) Normalized electroluminescence spectra. (b) EQE–luminance curves.

Concentration wt%	λ_{em} [nm]	FWHM [nm]/[meV]	CE_{max} [cd A^{-1}]	PE_{max} [lm W^{-1}]	EQE_{max}/EQE_{1000} [%]	CIE (x, y)
1	502	35/173	86.0	76.0	34.5/12.3	(0.12, 0.59)
3	511	38/177	120.5	105.2	37.8/17.2	(0.17, 0.67)
5	514	41/192	123.2	107.5	36.2/17.6	(0.19, 0.68)
7	515	44/203	130.3	105.0	34.3/13.1	(0.21, 0.68)

Table S5. Electroluminescence properties of the DOBNA-*p*-CzBN-based devices.

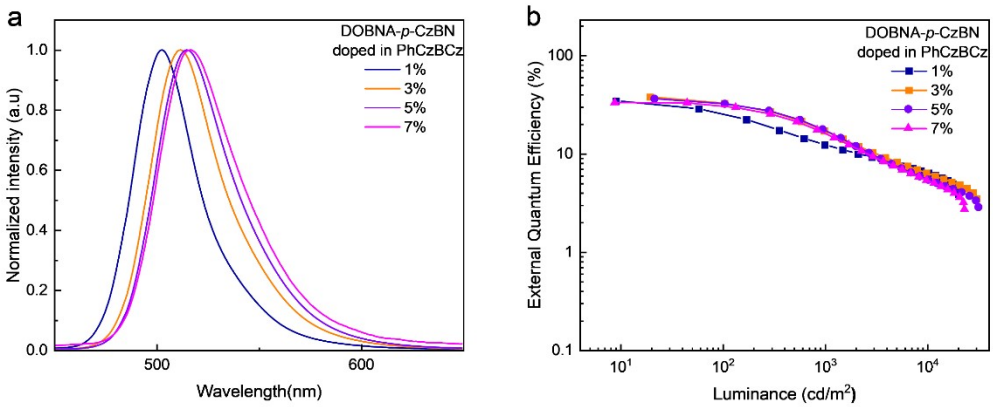

Figure S13. OLED device performances for DOBNA-*p*-CzBN with different doping concentrations. (a) Normalized electroluminescence spectrum. (b) EQE–luminance curves.

NMR Spectra.

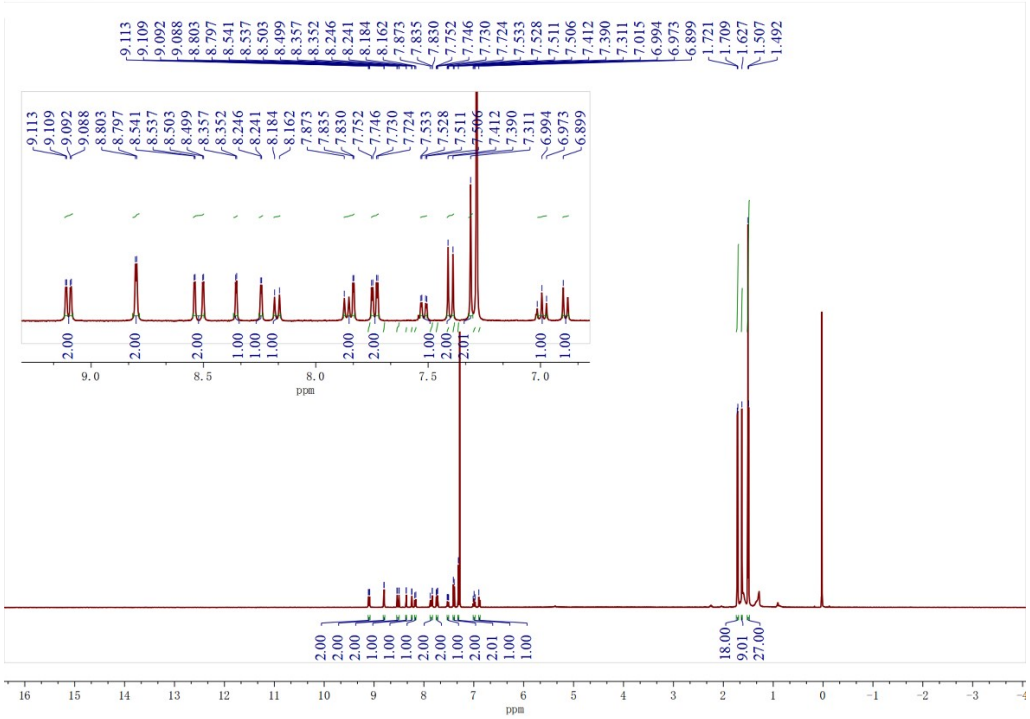

Figure S14. ^{1}H NMR spectrum of DOBNA-*m*-CzBN in Chloroform-*d*.

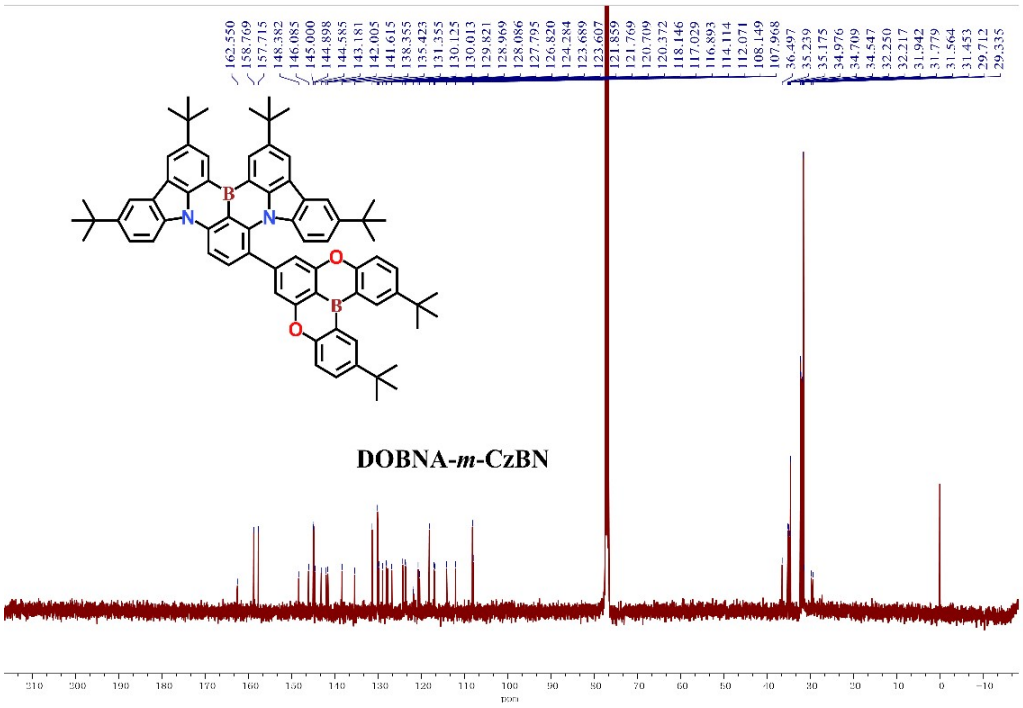

Figure S15. ^{13}C NMR spectrum of DOBNA-*m*-CzBN in Chloroform-*d*.

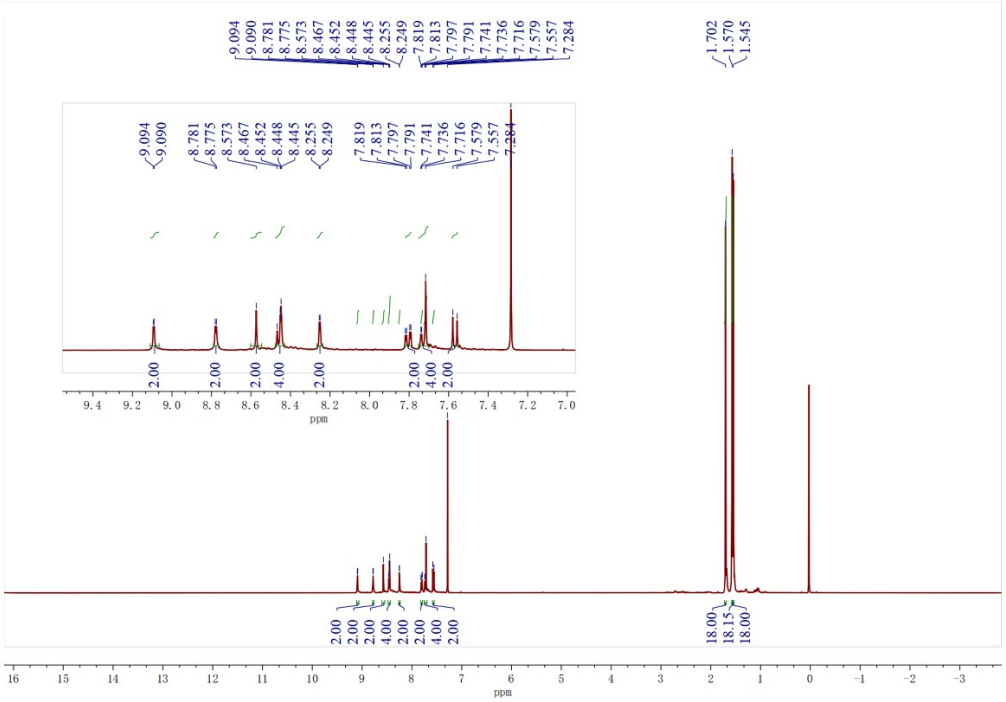

Figure S16. ^{1}H NMR spectrum of DOBNA-*p*-CzBN in Chloroform-*d*.

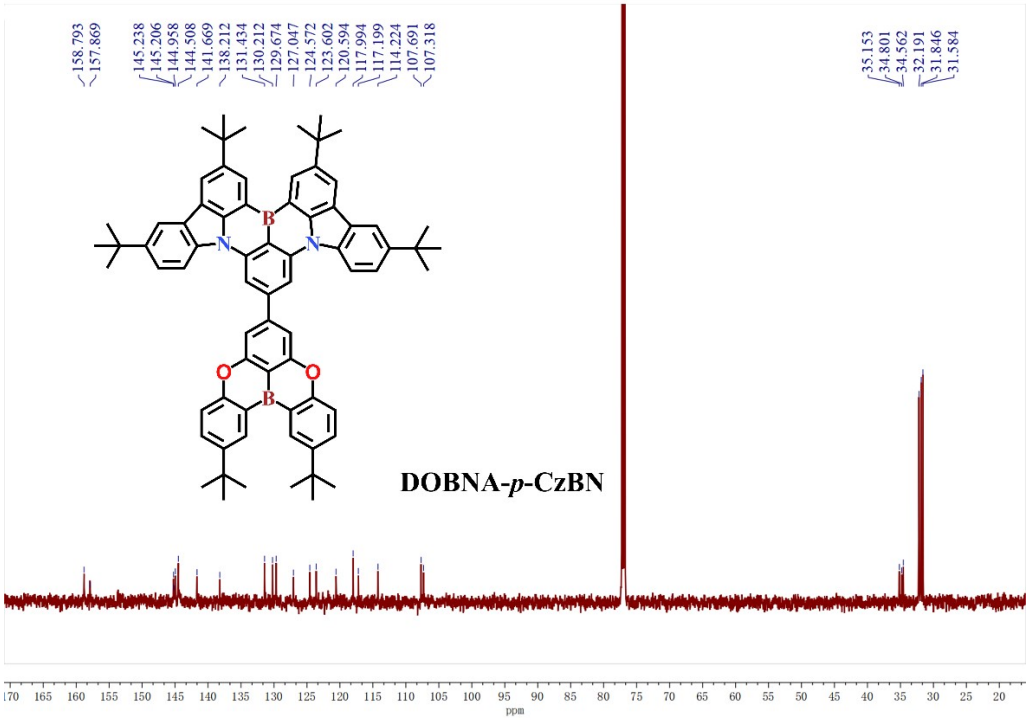

Figure S17. ^{13}C NMR spectrum of DOBNA-*p*-CzBN in Chloroform-*d*.

References

1. D. Karthik, D. H. Ahn, J. H. Ryu, H. Lee, J. H. Maeng, J. Y. Lee and J. H. Kwon, *J. Mater. Chem.*, 2020, **8**, 2272-2279.
2. F. Rauch, P. Endres, A. Friedrich, D. Sieh, M. Hahnel, I. Krummenacher, H. Braunschweig, M. Finze, L. Ji and T. B. Marder, *Chem. - Eur. J.*, 2020, **26**, 12951-12963.
3. Q. Y. Wang, Y. C. Xu, T. Yang, J. A. Xue and Y. Wang, *Adv. Mater.*, 2023, **35**, 2205166.
4. Y. Liu, X. Xiao, Y. Ran, Z. Y. Bin and J. S. You, *Chem. Sci.*, 2021, **12**, 9408-9412.
5. X. Qiu, G. J. Tian, C. W. Lin, Y. Y. Pan, X. Y. Ye, B. H. Wang, D. G. Ma, D. H. Hu, Y. Luo and Y. G. Ma, *Adv. Opt. Mater.*, 2021, **9**, 2001845.